PCCP

PAPER

View Article Online
View Journal | View Issue

Cite this: *Phys. Chem. Chem. Phys.*, 2024, **26**, 7371

Absence of superconductivity in *I*4/*mmm*-FeH_5: experimental evidence†

Yulong Wang,[a] Su Chen,[a] Jianning Guo,[a] Xiaoli Huang *[a] and Tian Cui [ab]

Received 9th December 2023,
Accepted 6th February 2024

DOI: 10.1039/d3cp05996k

rsc.li/pccp

The experimentally discovered FeH_5 exhibits a structure built of atomic hydrogen that only has bonding between hydrogen and iron atoms [C. M. Pepin, G. Geneste, A. Dewaele, M. Mezouar and P. Loubeyre, *Science*, 2017, **357**, 382]. However, its superconductivity has remained unsolved since its discovery. In this work, we have synthesized *I*4/*mmm*-FeH_5 at 139 GPa combined with laser-heating conditions. The electrical resistance measurements at ultrahigh pressures indicate that no evidence of superconducting transition of FeH_5 is observed in the temperature range of 1.5 K to 270 K. These results indicate that *I*4/*mmm*-FeH_5 does not exhibit superconductivity within the experimental temperature range, and the introduction of iron atoms is not beneficial to the formation of the superconducting phase.

Introduction

Hydrogen has been predicted to be a superconductor with high critical temperatures (T_c) at high pressures.[1] Theoretical calculations indicate that the T_c of hydrogen will exceed 240 K or even close to room temperature with a pressure above 500 GPa.[2–4] Although extensive research on hydrogen has been conducted, scientists have not obtained direct data in electrical transport experiments which can prove the metallization and superconductivity of solid hydrogen.[5–8] Encouragingly, Ashcroft predicted that the introduction of heavier elements would enhance intermolecular interactions between hydrogen. This process is known as "chemical precompression", which would have a positive impact and can realize the metallization and superconductivity of hydrogen at lower pressures.[9] For example, H_3S has a T_c of ~200 K at ~150 GPa[10–13] and LaH_{10} has a T_c of ~250 K at ~150 GPa.[14–17]

On the other hand, according to the observations in geomagnetism and seismology, iron is the most abundant element in the Earth's core.[18–20] However, if the Earth's core consists of pure iron, the density of it is ~2–5% more than reality at relevant pressures and temperatures.[21–25] Therefore, the Earth's core should have elements lighter than iron such as nickel (it is definable exist in the Earth's core), silicon, sulphur, oxygen, carbon and hydrogen.[22,26–28] The iron–water reaction, $Fe + O_2 \rightarrow FeH_x + FeO$, could take place at pressures and temperatures lower than the Earth's core, which means that iron hydrides are the prospective components of the Earth's core.[29–31] In this regard, conducting measurements of the mechanical, electrical, and magnetic properties of iron hydrides are of significant importance in exploring the Earth's core and gaining further insights into the Earth's structure. For example, FeH has been extensively studied: dhcp-FeH (ε'), which can be stable in excess of 62 GPa, has been synthesised at ~1000 °C and ~5 GPa;[19,32] two magnetic phase transitions of dhcp-FeH were found theoretically and experimentally at ~26 GPa and ~43 GPa, respectively.[25,33–36]

Concurrently, iron hydrides with a higher hydrogen content have been predicted or synthesized successively. In experiments, Gavriliuk *et al.* have synthesized *I*4/*mmm*-FeH_2 at 77 GPa and ~2000 K;[37] Pepin *et al.* have synthesized *I*4/*mmm*-FeH_2 and *Pm*-3*m*-FeH_3 at 67 GPa and 86 GPa after heating to ~1500 K, respectively,[38] and they also first detected *I*4/*mmm*-FeH_5 at ~150 GPa after heating to ~1500 K.[39] Gavriliuk *et al.* have synthesized new iron hydrides with possible T_c of ~25 K and 27.7 K at ~178 GPa and 195 GPa respectively; unfortunately, they did not determine their crystal structures.[40] Theoretically, several studies have reported new phases of the Fe–H system, including FeH_3,[41] FeH_4,[42] FeH_6[43–45] and FeH_7.[45] Most of these and some other iron hydrides are summarized in a phase diagram.[46] Among all the iron hydrides, *I*4/*mmm*-FeH_5 has the highest hydrogen content in experiments and a very particular structure with puckered hexagonal honeycomb layers. The H–H nearest-neighbour distance of *I*4/*mmm*-FeH_5 is 1.32 Å at 130 GPa and this phase only has bonding between hydrogen and iron atoms. So, *I*4/*mmm*-FeH_5 is regarded as a typical example of the "precompression". Some theoretical works have proposed that *I*4/*mmm*-FeH_5 is a potential superconductor with a T_c of ~ 50 K,[44,47,48] while others consider that FeH_5 is not a superconductor.[45,49] Considering the unique structure of FeH_5 and controversial calculated results, it is necessary to

[a] *State Key Laboratory of Superhard Materials, College of Physics, Jilin University, Changchun 130012, China*
[b] *School of Physical Science and Technology, Ningbo University, Ningbo, 315211, China. E-mail: huangxiaoli@jlu.edu.cn*

† Electronic supplementary information (ESI) available. See DOI: https://doi.org/10.1039/d3cp05996k

conduct experiments to explore its superconductivity and provide more clues for the high-temperature superconducting hydrides.

In this work, we have successfully synthesized FeH_5 by compression of Fe and NH_3BH_3 at high pressures with laser heating to ~1400 K. Electrical transport measurements indicate that FeH_5 retains a metallic character without transforming into the superconducting (SC) phase in the temperature range of 1.5–270 K.

Experimental details

We conducted three runs to investigate the superconductivity and structure of the Fe–H system at high pressure. Iron foil (purchased from Alfa Aesar, purity 99.99%) was pre-compressed and loaded into a diamond anvil cell (DAC) together with NH_3BH_3, which was used as the pressure-transmitting medium and hydrogen source.[15,50] For electrical resistance measurements, we used DACs made of NiCrAl alloy, and the diamonds had a culet of 50, 60, and 80 μm in diameter bevelled at 8° to a diameter of about 300 μm. A near-IR laser (YLR-200, 1070 nm) was used in our laboratory to heat the sample in the DAC with a spot size of ~5 μm.[51] The electrical resistance was measured using the four-probe method with the delta model of a Keithley current source (Model 6221) and a voltmeter (Model 2182A).[52,53] Mo electrodes were sputtered on the surface of diamond anvils to connect Pt electrodes and the sample, and MgO/epoxy was used as an insulating layer to separate the tungsten gasket and electrodes. The low temperature measurements were carried out in a helium cryostat (1.5–300 K) equipped with a 0–9 T superconducting magnet. The pressure was calibrated by the Raman shift of the diamond anvil.[54] All crystal structures were determined by *in situ* X-ray diffraction (XRD) on the beamline BL15U1 of the Shanghai synchrotron radiation facility (SSRF), with a wavelength of 0.6199 Å and a spot size of ~3 μm^2. The XRD patterns were analysed using Diopatas,[55] Jana2006[56] and GSAS-II.[57]

Results and discussion

Experimental results

We conducted three runs (cells #1–3) of electrical transport measurements on Fe–H compounds synthesized by laser heating at specific pressures. We have plotted the corresponding electrical resistance data during the cooling process in Fig. 1. In cell #1, three cycles of laser heating were carried out at 154, 160 and 164 GPa, respectively. Unfortunately, no superconducting transition was detected in the electrical resistance measurement apart from the drop of the electrodes (Fig. 1a). In cell #2 and cell #3, after heating the sample at the target pressures, no superconducting transition was detected except the drop of the electrodes as well (Fig. 1b and c).

To determine the possible phases produced in the electrical cell, we have performed the synchrotron X-ray diffraction measurements on the same sample. Considering the possibility of synthesising non-superconducting Fe–H phases during the first and second heating in cell #3, we obtained *in situ* XRD patterns at 143 GPa. The XRD results showed that the sample was still the pure $P6_3/mmc$-Fe phase and no FeH compound was generated (Fig. 2a). Therefore, a third laser heating was performed at 139 GPa. After XRD characterization, it was found that the

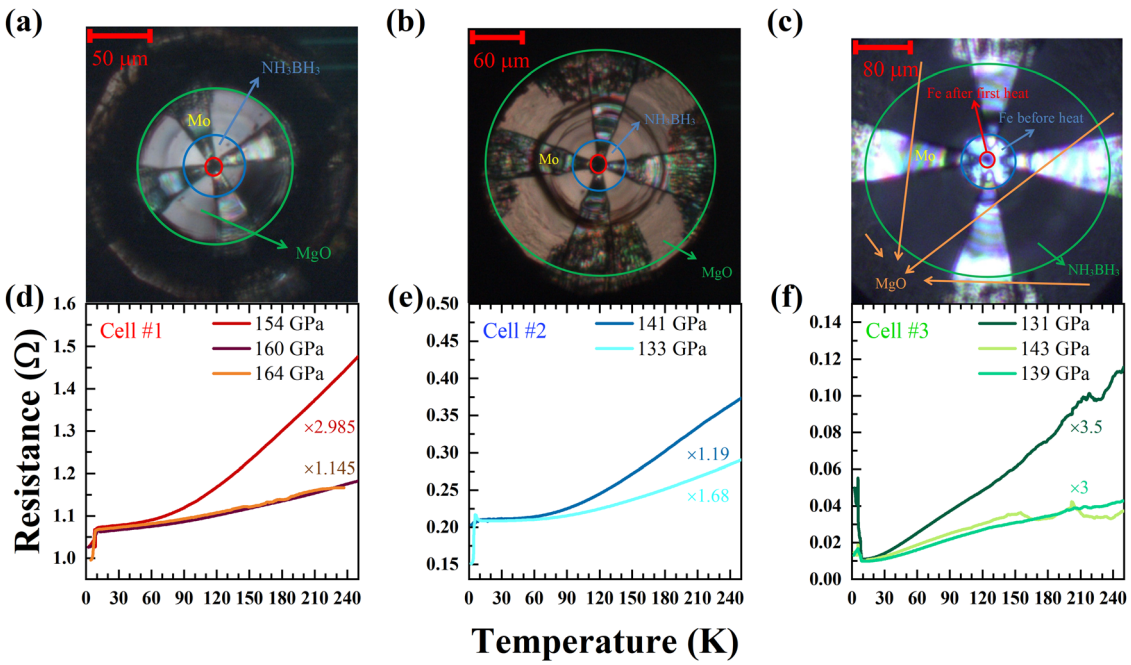

Fig. 1 Optical micrographs of the sample chamber and electrical transport measurements of the Fe–H sample at high pressures. (a)–(c) Photographs of cells after laser heating, and the edges of the sample are marked with red circles. (d)–(f) Resistance data in cell #1, cell #2, and cell #3, respectively. To compare trends and kinks in each curve easily, the resistance of the samples was multiplied by the marked values.

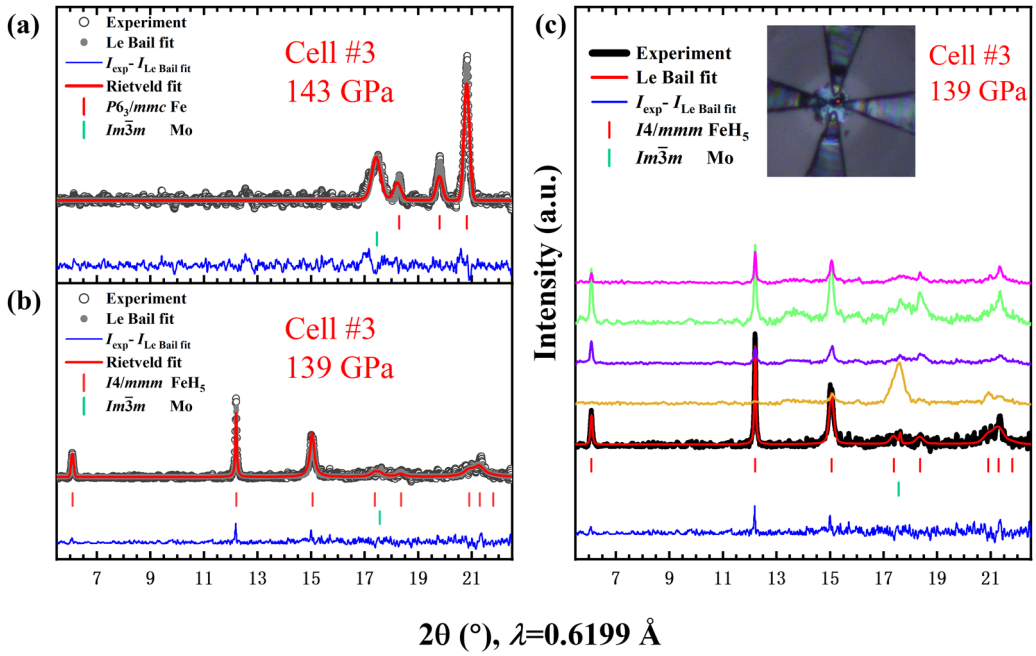

Fig. 2 Synchrotron X-ray diffraction (XRD) patterns (λ = 0.6199 Å) of the synthesized sample at high pressures. (a) XRD pattern of the sample before laser-heating at 143 GPa. The cell parameters of $P6_3/mmc$-Fe are $a = b$ = 2.2527 Å and c = 3.6053 Å. Grey hollow circles, grey solid circles, red lines and blue lines correspond to the experimental data, Le Bail fitted data, Rietveld fitted data and the difference of experimental and Le Bail fitted data, respectively. The signal of Mo electrodes in the bcc phase is also observed in the XRD pattern.[58,59] (b) XRD pattern of synthesized $I4/mmm$-FeH_5 at 139 GPa. (c) XRD patterns of the synthesized sample measured across the sample with a step of 3 μm. The red point indicates the initial laser focus position.

heated sample reacted with a large area (Fig. 2c) and generated the $I4/mmm$-FeH_5 phase (Fig. 2b), which was consistent with the previous work.[39] The cell parameters of $I4/mmm$-FeH_5 in this work at a pressure of 139 GPa are $a = b$ = 2.4172 Å, and c = 11.6647 Å. The crystal structures of $P6_3/mmc$-Fe and $I4/mmm$-FeH_5 are shown in Fig. 3a and b, and the refined lattice parameters and R-values in this work are shown in Table S1 (ESI†). $P6_3/mmc$-Fe is a typical hexagonal close packed (hcp) structure with an ABAB stacking of Fe layers. $I4/mmm$-FeH_5 exhibits a structure consisting of quasi-cubic FeH_3 unit layers and four-plane slabs of thin atomic hydrogen, and it can also be considered as a combination of Fe layers and puckered hexagonal honeycomb hydrogen layers. The comparison of the unit cell volume in Fig. 3c also certifies the synthesis of FeH_5 in agreement with ref. 39. However, after conducting electrical transport tests, it was found that there was no superconducting transition attributed to FeH_5 (Fig. 1c).

In addition, there is a small drop in 14 K at 143 GPa in cell #3, and to confirm whether the drop was the superconducting transition of FeH_5, the second cooling process was made; but unfortunately the result could not be repeated (Fig. S2, ESI†), and other cooling measurements had not detected the similar

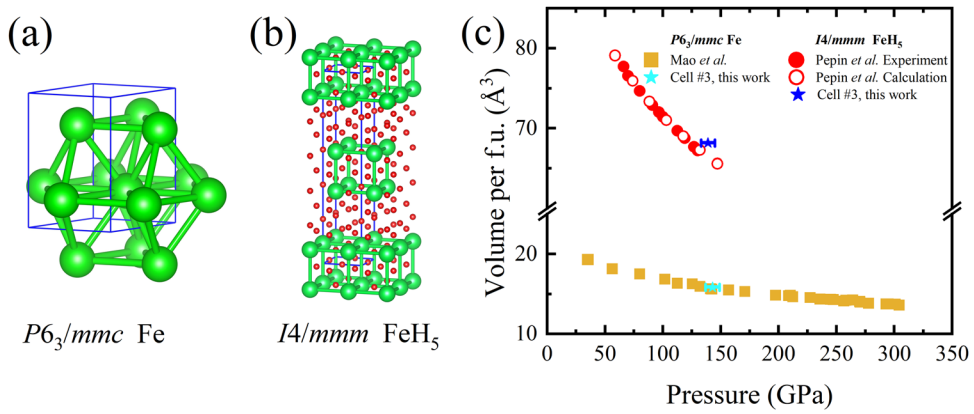

Fig. 3 Structures and pressure–volume data of the Fe–H samples at different pressures in cell #3. (a) and (b) Crystal structures of Fe and FeH_5, respectively. Green and red balls represent Fe and H atoms, respectively. (c) Pressure dependence of the unit cell volume (per f.u.). Brown solid squares and red solid and hollow circles represent the experimental data of $P6_3/mmc$-Fe from ref. 23 and the experimental and calculation data of $I4/mmm$-FeH_5 from ref. 39, respectively. Experimental data in this study are represented by solid stars with error bars of pressure.

signal yet. On the other hand, there are obvious some bends in the front of the curves. We attribute it to the superconducting transition of Mo electrodes or MoC_x because the diamonds were heated to ~1000 K to prepare the Mo electrodes in magnetron sputtering equipment. Another reason is that the Mo electrodes may react with diamonds in laser heating of the sample. Two curves, representing the resistance data of Fe and FeH_5 at 143 GPa and 139 GPa respectively, are put together to verify whether the bends are from the superconductivity of FeH_5 (Fig. S3, ESI†). Vertical reference lines indicate that all the bends of the resistance curve of FeH_5 can correspond to the curve of Fe, so they are not evidence of superconducting transitions of FeH_5.

In order to further confirm the change of the sample, the electrical resistance as a function of temperature at different pressures was fitted by the form of $R(T) = R_0 + AT^{\alpha}$,[60] where R_0 is the residual resistance and A and α are the coefficient of power function and the power exponent of temperature, respectively. After the first heating in cell #1 (154 GPa) and second heating in cell #3 (143 GPa), the low temperature resistance is related to the second power of temperature, indicating that the sample may not be reacted with hydrogen and remains pure iron obeying Fermi liquid theory (Fig. 4a and c). But as shown in Fig. 4b, α had a noticeable change after the second heating in cell #1 (160 GPa). Furthermore, the sample colour changed from metallic to black and a distinct Raman signal of hydrogen (see Fig. S1, ESI†) occurred after the third heating. All these phenomena point to the formation of new hydrides.[61,62] In Fig. 4a and b, the parameter α is changed from 2.027 to 0.980 after the second heating, probably indicating the strange metal (SM) character in the formed iron hydride.[63–65] And, in Fig. 4c and d, the parameter α is changed from 1.960 to 2.122 after the third heating, indicating that FeH_5 behaves like a normal metal corresponding to Fermi liquid theory. Future electrical transport measurements will provide more detailed information on various iron hydrides.

Discussion

Because the positions of H atoms cannot be determined by XRD experiments at high pressures, the bonds of H–H atoms are controversial. Pepin *et al.* consider that the structure of FeH_5 is similar to two-dimensional materials, in which Fe–H atoms form bonds while H–H atoms do not form bonds.[39] However, in some theoretical work, the structure of FeH_5 can be seen as two

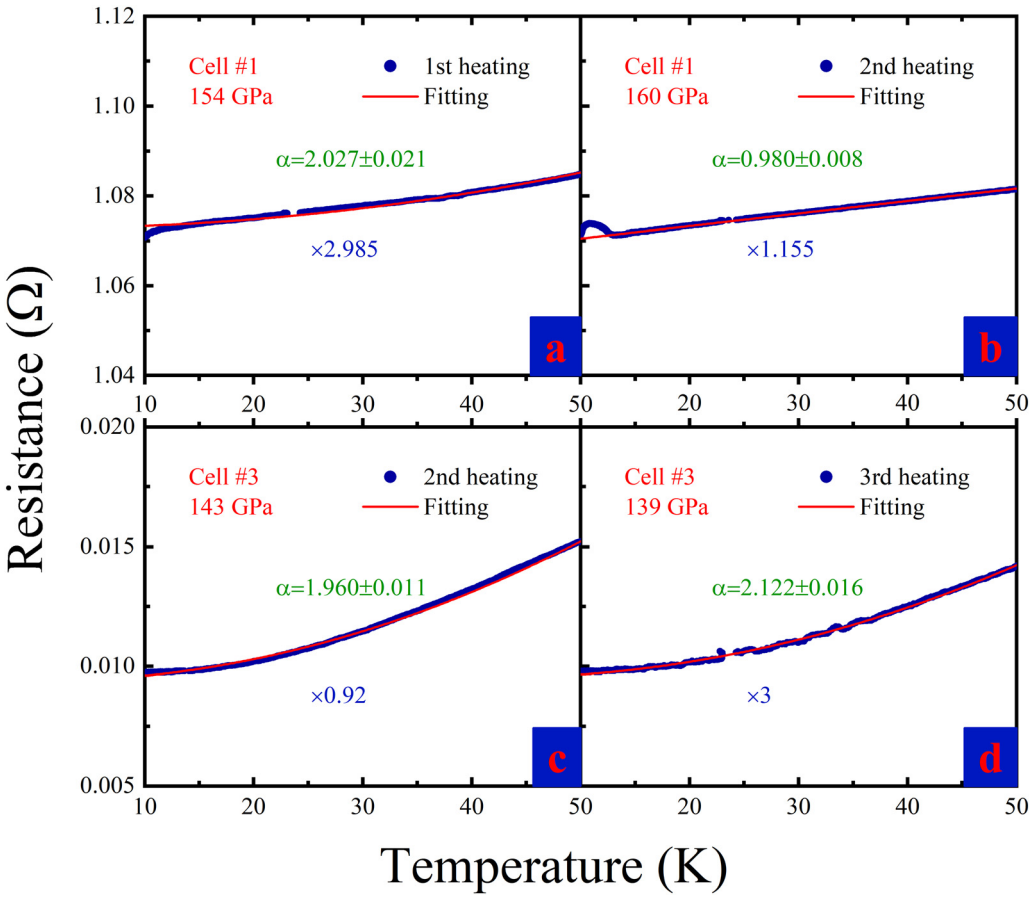

Fig. 4 Resistance as a function of temperature at different pressures and corresponding fits by the form of $R(T) = R_0 + AT^{\alpha}$. (a) and (b) The fitting of resistance data after the 1st heating (154 GPa) and 2nd heating (160 GPa) in cell #1. Data in curves are the actual data multiplied by a number as shown in blue marks. (c) and (d) The fitting of resistance data after the 2nd heating (143 GPa) and 3rd heating (139 GPa) in cell #3.

independent graphene-like puckered hexagonal honeycomb hydrogen atom layers inserted between iron atom layers, with weak electron localization between H atoms.[48,49] Furthermore, the high pressure hydrogen phase with the space group *Cmca* is similar to the *I*4/*mmm*-FeH_5 structure and the theoretical prediction reveals that *Cmca*-H_2 has a T_c of 242 K at 450 GPa.[2,66] And, it has also been predicted in hydrides that SrH_{10} with the similar structure has a T_c of 259 K. Because the puckered honeycomb layer structures have strong mixing of stretch and bent vibrations, strong electron–phonon coupling easily occurs and can increase the superconducting transition temperature.[67] But the superconductivity of *I*4/*mmm*-FeH_5 is controversial. Some theoretical works predicted that FeH_5 has a T_c of $\sim$50 K at $\sim$150 GPa,[44,47,48] but others consider that FeH_5 is not a superconductor.[45,49] Although conclusions are different, there are some similarities in their theoretical calculations, and it can be seen from the density of electron states and phonon states.[44,45,47–49] The electrons of iron atoms play a major role near the Fermi surface; the only band with appreciable Fe–H hybridization and electron–phonon (*e*-ph) coupling lies above the Fermi level rather than near the Fermi level; for the phonon modes below 650 cm^{-1}, iron still plays a dominant role and contributes the most to the *e*-ph coupling interaction. In summary, FeH_5 behaves just like elemental metals rather than other high T_c superconducting hydrides in band structure like H_3S and LaH_{10}, and exhibits a strong *e*-ph coupling near the Fermi level and hydrogen plays a dominant role in phonon density of states (PHDOS).[12,17] So, it is obvious that the introduction of iron atoms cannot benefit superconductivity with similar structures compared with pure solid hydrogen.

Conclusions

In conclusion, we have successfully synthesized FeH_5 by compression of Fe and NH_3BH_3 at 139 GPa with laser heating to about 1400 K. The refined XRD results confirmed the crystal structure of FeH_5 as reported in the *I*4/*mmm*-FeH_5 phase, and no superconductivity evidence is observed in electrical transport measurements within the range of 1.5–270 K. Through function fitting in low temperature resistance, FeH_5 behaves as a typical metal in consistent with Fermi liquid theory. Our results indicate that the chemical precompression of iron atoms is not beneficial to the superconductivity even though it has a similar structure to pure atomic hydrogen. We hope that this work can end the debate on the superconductivity of FeH_5 and provide more insights into the study of superconducting transition metal hydrides.

Data availability

The authors declare that the main data supporting the findings of this study are contained within the paper and its associated ESI.† All other relevant data are available from the corresponding author upon reasonable request.

Conflicts of interest

There are no conflicts to declare.

Acknowledgements

This work was supported by the National Natural Science Foundation of China under grant numbers 52372257 and 52072188, the Program for Changjiang Scholars and Innovative Research Team in University under the grant number IRT_15R23, the Zhejiang Provincial Science and technology innovation Team under the grant number 2021R01004, and the Fundamental Research Funds for the Central Universities. The authors thank the staff of the Shanghai Synchrotron Radiation Facility for their help during the synchrotron XRD measurements.

References

1 N. W. Ashcroft, *Phys. Rev. Lett.*, 1968, **21**, 1748–1749.
2 P. Cudazzo, G. Profeta, A. Sanna, A. Floris, A. Continenza, S. Massidda and E. K. U. Gross, *Phys. Rev. Lett.*, 2008, **100**, 257001.
3 J. M. McMahon and D. M. Ceperley, *Phys. Rev. B: Condens. Matter Mater. Phys.*, 2011, **84**, 144515.
4 M. Borinaga, I. Errea, M. Calandra, F. Mauri and A. Bergara, *Phys. Rev. B*, 2016, **93**, 174308.
5 P. Loubeyre, F. Occelli and P. Dumas, *Nature*, 2020, **577**, 631–635.
6 M. I. Eremets and I. A. Troyan, *Nat. Mater.*, 2011, **10**, 927–931.
7 R. P. Dias and I. F. Silvera, *Science*, 2017, **355**, 715–718.
8 D. Castelvecchi, *Nature*, 2017, **542**, 17.
9 N. W. Ashcroft, *Phys. Rev. Lett.*, 2004, **92**, 187002.
10 A. P. Drozdov, M. I. Eremets, I. A. Troyan, V. Ksenofontov and S. I. Shylin, *Nature*, 2015, **525**, 73–76.
11 X. Huang, X. Wang, D. Duan, B. Sundqvist, X. Li, Y. Huang, H. Yu, F. Li, Q. Zhou, B. Liu and T. Cui, *Natl. Sci. Rev.*, 2019, **6**, 713–718.
12 D. Duan, Y. Liu, F. Tian, D. Li, X. Huang, Z. Zhao, H. Yu, B. Liu, W. Tian and T. Cui, *Sci. Rep.*, 2014, **4**, 6968.
13 M. Einaga, M. Sakata, T. Ishikawa, K. Shimizu, M. I. Eremets, A. P. Drozdov, I. A. Troyan, N. Hirao and Y. Ohishi, *Nat. Phys.*, 2016, **12**, 835–838.
14 A. P. Drozdov, P. P. Kong, V. S. Minkov, S. P. Besedin, M. A. Kuzovnikov, S. Mozaffari, L. Balicas, F. F. Balakirev, D. E. Graf, V. B. Prakapenka, E. Greenberg, D. A. Knyazev, M. Tkacz and M. I. Eremets, *Nature*, 2019, **569**, 528–531.
15 M. Somayazulu, M. Ahart, A. K. Mishra, Z. M. Geballe, M. Baldini, Y. Meng, V. V. Struzhkin and R. J. Hemley, *Phys. Rev. Lett.*, 2019, **122**, 027001.
16 F. Peng, Y. Sun, C. J. Pickard, R. J. Needs, Q. Wu and Y. Ma, *Phys. Rev. Lett.*, 2017, **119**, 107001.
17 H. Liu, I. I. Naumov, R. Hoffmann, N. W. Ashcroft and R. J. Hemley, *Proc. Natl. Acad. Sci. U. S. A.*, 2017, **114**, 6990–6995.
18 D. J. Stevenson, *Science*, 1981, **214**, 611–619.
19 Q. Williams and R. Jeanloz, *J. Geophys. Res.*, 1990, **95**, 19299–19310.

20 R. Jeanloz, *Annu. Rev. Earth Planet. Sci.*, 1990, **18**, 357–386.
21 A. F. Birch, *J. Geophys. Res.*, 1952, **57**, 227–286.
22 F. Birch, *J. Geophys. Res.*, 1964, **69**, 4377–4388.
23 H. K. Mao, Y. Wu, L. C. Chen, J. F. Shu and A. P. Jephcoat, *J. Geophys. Res.*, 1990, **95**, 21737–21742.
24 E. I. Isaev, N. V. Skorodumova, R. Ahuja, Y. K. Vekilov and B. Johansson, *Proc. Natl. Acad. Sci. U. S. A.*, 2007, **104**, 9168–9171.
25 N. Hirao, T. Kondo, E. Ohtani, K. Takemura and T. Kikegawa, *Geophys. Res. Lett.*, 2004, **31**, L06616.
26 J.-P. Poirier, *Phys. Earth Planet. Inter.*, 1994, **85**, 319–337.
27 K. Hirose, S. Labrosse and J. Hernlund, *Annu. Rev. Earth Planet. Sci.*, 2013, **41**, 657–691.
28 A. E. Ringwood, *Proc. Math. Phys. Eng. Sci.*, 1984, **395**, 1–46.
29 Y. Fukai, *Nature*, 1984, **308**, 174–175.
30 T. Suzuki, S.-i Akimoto and Y. Fukai, *Phys. Earth Planet. Inter.*, 1984, **36**, 135–144.
31 E. Ohtani, N. Hirao, T. Kondo, M. Ito and T. Kikegawa, *Phys. Chem. Miner.*, 2005, **32**, 77–82.
32 J. V. Badding, R. J. Hemley and H. K. Mao, *Science*, 1991, **253**, 421–424.
33 V. E. Antonov, I. T. Belash, E. G. Ponyatovskii, V. G. Thiessen and V. I. Shiryaev, *Phys. Status Solidi A*, 1981, **65**, K43–K48.
34 T. Tsumuraya, Y. Matsuura, T. Shishidou and T. Oguchi, *J. Phys. Soc. Jpn.*, 2012, **81**, 064707.
35 N. Bouldi, P. Sainctavit, A. Juhin, L. Nataf and F. Baudelet, *Phys. Rev. B*, 2018, **98**, 064430.
36 J. Ying, J. Zhao, W. Bi, E. E. Alp, Y. Xiao, P. Chow, G. Shen and V. V. Struzhkin, *Phys. Rev. B*, 2020, **101**, 020405.
37 A. G. Gavriliuk, V. V. Struzhkin, S. N. Aksenov, A. G. Ivanova, A. A. Mironovich, I. A. Troyan and I. S. Lyubutin, *JETP Lett.*, 2023, **116**, 804–816.
38 C. M. Pepin, A. Dewaele, G. Geneste, P. Loubeyre and M. Mezouar, *Phys. Rev. Lett.*, 2014, **113**, 265504.
39 C. M. Pepin, G. Geneste, A. Dewaele, M. Mezouar and P. Loubeyre, *Science*, 2017, **357**, 382.
40 A. G. Gavriliuk, I. A. Troyan, V. V. Struzhkin, D. N. Trunov, S. N. Aksenov, A. A. Mironovich, A. G. Ivanova and I. S. Lyubutin, *JETP Lett.*, 2023, **118**, 742–753.
41 Z. G. Bazhanova, A. R. Oganov and O. Gianola, *Phys.-Usp.*, 2012, **55**, 489–497.
42 F. Li, D. Wang, H. Du, D. Zhou, Y. Ma and Y. Liu, *RSC Adv.*, 2017, **7**, 12570–12575.
43 S. Zhang, J. Lin, Y. Wang, G. Yang, A. Bergara and Y. Ma, *J. Phys. Chem. C*, 2018, **122**, 12022–12028.
44 A. G. Kvashnin, I. A. Kruglov, D. V. Semenok and A. R. Oganov, *J. Phys. Chem. C*, 2018, **122**, 4731–4736.
45 N. Zarifi, T. Bi, H. Liu and E. Zurek, *J. Phys. Chem. C*, 2018, **122**, 24262–24269.
46 D. N. Sagatova, P. N. Gavryushkin, N. E. Sagatov, I. V. Medrish and K. D. Litasov, *JETP Lett.*, 2020, **111**, 145–150.
47 K. M. Skoczylas, A. P. Durajski and R. Szczęśniak, *Phys. B*, 2020, **584**, 412063.
48 A. Majumdar, J. S. Tse, M. Wu and Y. Yao, *Phys. Rev. B*, 2017, **96**, 201107.
49 C. Heil, G. B. Bachelet and L. Boeri, *Phys. Rev. B*, 2018, **97**, 214510.
50 Y. V. Kondrat'ev, A. V. Butlak, I. V. Kazakov and A. Y. Timoshkin, *Thermochim. Acta*, 2015, **622**, 64–71.
51 S. Anzellini and S. Boccato, *Crystals*, 2020, **10**, 459.
52 D. Errandonea, E. Bandiello, A. Segura, J. J. Hamlin, M. B. Maple, P. Rodriguez-Hernandez and A. Muñoz, *J. Alloys Compd.*, 2014, **587**, 14–20.
53 B. Wu, Y. Han, G. Peng, X. Huang, C. Liu, F. Jin and C. Gao, *Phys. Status Solidi C*, 2011, **8**, 1692–1694.
54 Y. Akahama and H. Kawamura, *J. Appl. Phys.*, 2006, **100**, 043516.
55 C. Prescher and V. B. Prakapenka, *High Press. Res.*, 2015, **35**, 223–230.
56 V. Petříček, M. Dušek and L. Palatinus, *Z. Kristallogr. – Cryst. Mater.*, 2014, **229**, 345–352.
57 B. H. Toby and R. B. Von Dreele, *J. Appl. Crystallogr.*, 2013, **46**, 544–549.
58 Y. Akahama, N. Hirao, Y. Ohishi and A. K. Singh, *J. Appl. Phys.*, 2014, **116**, 223504.
59 J. Wang, F. Coppari, R. F. Smith, J. H. Eggert, A. E. Lazicki, D. E. Fratanduono, J. R. Rygg, T. R. Boehly, G. W. Collins and T. S. Duffy, *Phys. Rev. B*, 2016, **94**, 104102.
60 S. Cai, J. Zhao, N. Ni, J. Guo, R. Yang, P. Wang, J. Han, S. Long, Y. Zhou, Q. Wu, X. Qiu, T. Xiang, R. J. Cava and L. Sun, *Nat. Commun.*, 2023, **14**, 3116.
61 V. Schettino, R. Bini, M. Ceppatelli, L. Ciabini and M. Citroni, in *Adv. Chem. Phys.*, ed. S. A. Rice, John Wiley & Sons, Inc, Hoboken, NJ, USA, 2005, vol. 131, pp. 105–242.
62 D. Errandonea, *J. Phys. Chem. Solids*, 2009, **70**, 1117–1120.
63 S. Martin, A. T. Fiory, R. M. Fleming, L. F. Schneemeyer and J. V. Waszczak, *Phys. Rev. Lett.*, 1988, **60**, 2194–2197.
64 S. Martin, A. T. Fiory, R. M. Fleming, L. F. Schneemeyer and J. V. Waszczak, *Phys. Rev. B: Condens. Matter Mater. Phys.*, 1990, **41**, 846–849.
65 G. S. Boebinger, *Science*, 2009, **323**, 590–591.
66 C. J. Pickard and R. J. Needs, *Nat. Phys.*, 2007, **3**, 473–476.
67 K. Tanaka, J. S. Tse and H. Liu, *Phys. Rev. B*, 2017, **96**, 100502.

